Assessing Molecular Doping Efficiency in Organic Semiconductors with Reactive Monte Carlo

Archana Verma[1] and Nicholas E. Jackson[2]
[1)]*Department of Chemical and Biomolecular Engineering, University of Illinois Urbana-Champaign*
[2)]*Department of Chemistry, University of Illinois Urbana-Champaign*

(*Electronic mail: jacksonn@illinois.edu)

(Dated: January 14, 2024)

The addition of molecular dopants into organic semiconductors (OSCs) is a ubiquitous augmentation strategy to enhance the electrical conductivity of OSCs. Although the importance of optimizing OSC-dopant interactions is well-recognized, chemically generalizable structure-function relationships are difficult to extract due to the sensitivity and dependence of doping efficiency to chemistry, processing conditions, and morphology. Computational modelling for integrated OSC-dopant design is an attractive approach to systematically isolate fundamental relationships, but requires the challenging simultaneous treatment of molecular reactivity and morphology evolution. We present the first computational study to couple molecular reactivity with morphology evolution in a molecularly-doped OSC. Reactive Monte Carlo is employed to examine the evolution of OSC-dopant morphologies and doping efficiency with respect to dielectric, the thermodynamic driving for the doping reaction, and dopant aggregation. We observe that for well-mixed systems with experimentally relevant dielectric constants, doping efficiency is near unity with a very weak dependence on the ionization potential and electron affinity of OSC and dopant, respectively. At experimental dielectric constants, reaction-induced aggregation is observed, corresponding to the well-known insolubility of solution-doped materials. Simulations are qualitatively consistent with a number of experimental studies showing a decrease of doping efficiency with increasing dopant concentration. Finally, we observe that the aggregation of dopants lowers doping efficiency, and thus presents a rational design strategy for maximizing doping efficiency in molecularly doped OSCs. This work represents an important first step towards the systematic integration of molecular reactivity and morphology evolution into the characterization of multi-scale structure-function relationships in molecularly doped OSCs.

I. INTRODUCTION

Semiconducting materials have enabled the modern electronics industry, with electronic doping forming a cornerstone of practical silicon-based semiconductor devices. However, the applicability of inorganic semiconductors to large area optoelectronic devices is limited by high production costs and mechanical rigidity.[1] Organic semiconductors (OSCs) have emerged as promising materials for driving the development of cheap, solution-processable, lightweight, and flexible electronic devices. Currently, OSCs have been successfully commercialized as light-emitting diode materials in display and lighting technologies.[2,3] However, their broader commercial viability in applications such as transistors and photovoltaics is yet to be achieved.[4]

The physics of electronic doping in OSCs is subject to structural and energetic disorder,[5] which stands in contrast to doping in crystalline inorganic semiconductors. The doping mechanism in OSCs is generally accepted to involve two steps: charge transfer (ionization) and charge transport (dissociation). More specifically, in OSCs, ionization can result in two types of charge transfer states: integer charge transfer (ICT) or charge transfer complex (CTC) state formation. ICT states involve the transfer of an electron and consequent generation of a hole between an OSC-dopant pair. CTC state formation involves the hybridization of the frontier orbitals of the OSC and dopant; this net neutral complex requires subsequent thermal ionization by electronic excitation of an adjacent neutral OSC molecule to contribute to charge conductivity. Although the fully charge separated nature of ICT states is associated with higher conductivity than that of CTC states, only 5% of ICT states are able to dissociate and mobilize, due to the low dielectric constant of organic films resulting in strong electrostatic interactions between ionized molecules.[6]

A further complication unique to engineering doped OSC systems is that the the dopant concentrations required for OSCs (1%) are significantly higher than those for inorganic semiconductors (10^{-5}%), which leads to alterations in film morphology and a deterioration in performance. Concentration dependent trends are complicated by the confluence of increased generation of charge carriers, the simultaneous generation of Coulomb traps, disruptions of morphology, and the propensity for molecular aggregation.[7–9] The chemical and structural origin of dopant induced effects is particularly difficult to pinpoint in the ultralow concentration regime, as these trace chemical impurities often evade traditional microscopic, spectroscopic, and diffraction measurement detection limits.[5] Therefore, it is crucial to understand how dopant concentration affects morphology and impacts electrical conductivity, a metric of performance.[10,11]

Extensive experimental work has led to a large chemical space that impedes defining structure-property relationships. Target properties for optimization across chemistries include the highest occupied molecular orbital (HOMO) and lowest unoccupied molecular orbital (LUMO) energies, the degree of charge transfer, the dopant-OSC packing distance, and miscibility, among others.[4,5,12–15] Seemingly minor modifications to OSC-dopant systems commonly manifest as large changes in the dopant-OSC interface area, connectivity of OSC chains, dopant diffusivity, and processing attributes.[4,14,16–21] Importantly, the ratio of ICT to CTC states has been engineered

through such modifications in solvent, processing conditions, and relative position of OSC and dopant molecules.[16,22–26] Moreover, the limited miscibility of dopants in OSCs has been of particular importance as dopant aggregation and phase separation limit charge transfer and reduce both the doping efficiency and conductivity. Due to these complex interplays of length scales, reconciling the properties that comprise an effective dopant requires simultaneous consideration of the local morphology dependence of electronic energetics and structural disorder at the mesoscale.

Molecular simulations offer the potential to clarify how molecular modifications affect the electronic structure and morphology of doped OSC films. Absent from existing computational work on doped OSCs are methods that incorporate the strong coupling between OSC-dopant reactivity and the associated morphology. While molecular dynamics (MD) and Monte Carlo (MC) approaches to morphology evolution are powerful, they rarely (or at great computational cost) exhibit coupling to the underlying electronic structure of the system. Coarse graining can capture mesoscale morphology changes, for example in bulk heterojunctions[27,28], by simplifying molecular representations to improve computational scalability. However these simplifications are typically unable to reproduce the unique functionalities of OSC molecules which arise from directional interactions (such as $\pi-\pi$ stacking) and the sensitivity to local electronic structure (such as predicting ICT/CTC states).[29–31] By contrast, quantum chemical (QC) methods that take into account molecular reactivity cannot couple dynamically changing environmental information into the associated reactivity estimation at the necessary timescales of morphology evolution. Local energetics of OSC-dopant systems have been investigated using density functional theory (DFT) and all-atom MD, focusing on the propensity of molecules to form ICT/CTC states, rates of charge transfer, and rates of interconversion between ICT/CTC states.[1,22,24,32–35] However, these calculations are limited in scale, as high-accuracy electronic structure descriptions come at the expense of restricted system size. Molecular doping in OSCs stands at the interface of these two challenges where understanding of both the morphology dependence of doping and the doping dependence of the morphology are entirely lacking while being dependent on this strong coupling between simulation methodologies.

To properly treat this challenging computational approach, new methods that can incorporate electronic reactivity and morphology evolution within the full conformational ensemble are critical to making progress OSC-dopant systems. In this work, we establish a simple computational model which captures this strong coupling between molecular reactivity and multiscale morphology in molecularly doped OSCs. We adapt existing Reactive MC methodologies[36,37] to perform semigrand MC simulations of the full reactively coupled ensemble for molecular dopants. We employ this simple model to characterize the effects of the doping reaction free energy change, system density, dielectric constant, and dopant aggregation on the doping efficiency and morphology evolution of OSC-dopant systems.

The remainder of the paper is organized as follows. First, we describe the MC methodologies used and their experimentally motivated parameters. We then present our results and discuss their relevance to the broader OSC community. We conclude with a perspective towards future directions for strongly coupled models of reactivity and morphological evolution in doped OSCs.

II. METHODS

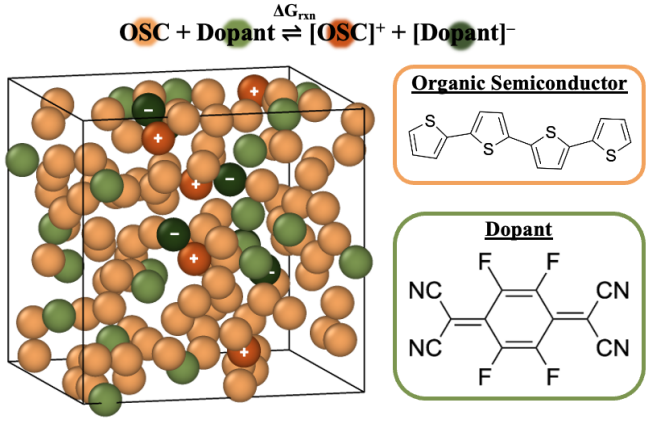

Figure 1. Simulation snapshot of neutral and cationic organic semiconductors, as well as neutral and anionic dopant particles, which interchange identities according to a doping reaction defined by Equation 1. The range of simulation parameters employed in this work are motivated by those of quarterthiophene and 2,3,5,6-tetrafluorotetracyanoquinodimethane, but are meant as a general exploration of chemically agnostic OSC-dopant morphologies.

We develop a simple MC model in which molecular OSC and dopant particles are treated as isotropic Lennard-Jones (LJ) beads that undergo translational, identity swap,[38–40] or reactive MC moves[36,37] to achieve chemical and configurational equilibration. System parameters, described in further detail in the subsequent section, were based on approximate experimentally known values for F4TCNQ doped thiophene films.[1,24,41–43] Each MC move proposal type is chosen with a predefined probability (0.2 for reactive moves, 0.2 for swap moves, and 0.6 for translational moves). Translational moves occur with a maximum displacement of 0.5σ drawn from a uniform distribution. Swap moves[38,39,44] were introduced to expedite equilibration in dense systems; we make the simplifying assumption that all particle types are of the same size σ, leading to a trivial implementation of the associated swap moves as identity swaps. Like swap moves, the reactive moves also enable the interconversion of species identity within a semigrand ensemble, although reactive moves do not necessarily conserve species populations and are rather governed by the stoichiometry of the reaction, as well as have an associated intrinsic free energy difference. A brief derivation of our MC simulation approach, and associated acceptance criteria, is provided below and is in accord with prior reactive MC frameworks.[36,37] Reactive moves are defined by the

following reaction equilibrium:

$$\text{Dopant} + \text{OSC} \overset{\Delta G_{rxn}}{\rightleftharpoons} \text{Dopant}^- + \text{OSC}^+ \tag{1}$$

This reaction assumes that the dominant charge carrier in the system is a hole, which is always localized on a single OSC molecule, consistent with the definition of an ICT state in the doping literature. This reaction is governed by a free-energy change, ΔG_{rxn}.

The probability within the grand canonical ensemble of being in a state r with N distinguishable particles is given by Equation 2.

$$P_r = \frac{1}{\Xi} exp[\Sigma_{i=1}^{c}(\beta N_i \mu_i + N_i ln(q_i)) - \beta U_r] \tag{2}$$

where Ξ is the grand canonical partition function, N_i is the number of particles in the system in state r, q_i is the single molecule partition function of species i, β is $1/k_B T$, μ_i is the chemical potential of species i, c denotes all species present in Equation 1, and U_r is the intermolecular potential energy of the system. The analogous expression for state s can be written as Equation 3, where the number of particles in the system at state s is given by the number of particles in the system in state r plus its associated stoichiometric coefficient (ν_i).

$$P_s = \frac{1}{\Xi} exp[\Sigma_{i=1}^{c}(\beta(N_i + \nu_i)\mu_i + (N_i + \nu_i) ln(q_i)) - \beta U_s] \tag{3}$$

Note that for the reaction defined by Equation 1, $\nu_i = 1$. The relative probability of state r and state s is given by the quotient of P_r and P_s. Noting that at equilibrium $\Sigma_{i=1}^{c} \nu_i \mu_i = 0$, we obtain Equation 4.

$$\frac{P_r}{P_s} = e^{-\beta \Delta U} \Pi_{i=1}^{c} q_i^{\nu_i} \tag{4}$$

where ΔU represents the change in the sytem's potential energy in going from state r to state s. We then factor out the ideal gas contribution to q_i, substituting $q_i = \frac{V}{\Lambda^3} q_{i,int}$ into Equation 4, where $q_{i,int}$ represents the internal (non-translational) contributions to the single molecule partition function of species i, V is the system volume, and Λ is the thermal de Broglie wavelength. Using the definition of the ideal gas equilibrium constant, $K^{ig}(T)$

$$\Pi_{i=1}^{c} (\frac{q_{i,int}}{\Lambda_i^3})^{\nu_i} = K^{ig}(T) \tag{5}$$

and the stoichiometric coefficients of Equation 1, we can simply cast Equation 4 as

$$\frac{P_r}{P_s} = e^{-\beta \Delta U} K^{ig}(T) \tag{6}$$

Relating the equilibrium constant to the single molecule contributions to the free energy of reaction, ΔG_{rxn}, the probability ratio of Eqn. 7 becomes simply:

$$\frac{P_r}{P_s} = exp[-\beta(\Delta U + \Delta G_{rxn})] \tag{7}$$

This probability ratio enables MC sampling of the semigrand ensemble. Configurational space sampling in this work is achieved with a combination of translational moves and identity swaps following standard Metropolis protocols. Forward and backward MC reaction move proposals (α_{rs} for the doping direction, α_{sr} for the de-doping direction) are obtained by enforcing detailed balance ($P_r \alpha_{rs} = P_s \alpha_{sr}$) with the following definitions for α_{rs} and α_{sr} (Eqn. 9).

$$\alpha_{rs} = \frac{1}{N_{Dopant} N_{OSC}} \tag{8}$$

$$\alpha_{sr} = \frac{1}{(N_{Dopant^-} + 1)(N_{OSC^+} + 1)} \tag{9}$$

Combining the transition probability (Eqn. 7) with the move proposal probabilities (Eqn. 9) yields the governing acceptance criterion in Equation 10.

$$p = min\{1, e^{-\beta(\Delta U_{LJ} + \Delta U_{ES} + \Delta G_{rxn})} \frac{N_{Dopant} N_{OSC}}{(N_{Dopant^-} + 1)(N_{OSC^+} + 1)}\} \tag{10}$$

where we have decomposed the intermolecular potential energy, ΔU, from Equation 7 into a sum of potential energy changes arising from classical electrostatics (ΔU_{ES}) and Lennard Jones interactions (ΔU_{LJ}), as is standard in classical force-fields. This acceptance criterion is equivalent to the semigrand canonical ensemble acceptance criterion due to the stoichiometry constraint on the doping reaction defined by Equation 1.[45]

Equation 13 is the critical expression for the presented MC method; the thermodynamic acceptance criterion for configurational and reaction moves explicitly couples molecularly specific reaction energies (ΔG_{rxn}) with multi-molecule electrostatic energies (ΔU_{ES}). The latter depends sensitively on the morphology of charged species. This approximation is the important enabling element for coupling molecular reactivity with morphology that can influence doping. Moreover, mutual solubility between OSC and dopant can be modulated via ΔU_{LJ}, which is tunable via the selection of OSC and dopant Lennard-Jones parameters.

As the present work assumes all doping reactions to be of the ICT type, where a single positive or negative charge is localized on a single OSC or dopant molecule, respectively, ΔG_{rxn} characterizes the thermodynamic driving force of this localized doping reaction. ΔG_{rxn} in the ionization (forward) direction is equivalent to the difference in free energies of the charged and neutral OSC and dopant species.

$$\Delta G_{rxn} = G_{final} - G_{initial} = G(D^- O^+) - G(DO) \quad (11)$$

While in principle, computing ΔG_{rxn} with this expression necessitates the inclusion of complex, often quantum-mechanical, multi-molecule effects, we utilize the simplifying single-molecule approximation present in our definition of the ideal gas equilibrium constant of Equation 5. Specifically, we rewrite ΔG_{rxn} within a single molecule approximation

$$\Delta G_{rxn} = (G(O^+) - G(O)) - (G(D^-) - G(D)) \quad (12)$$

Note that all intermolecular electrostatic interactions between charged species that are neglected in going from Equation 11 to Equation 12 are accounted for in the ΔU_{ES} term present in the decomposition of the intermolecular potential energy specified by Equation 10. Consequently, Coulombic interactions between charge carriers are properly accounted for, and not double counted, in our simulations. Note that for a single OSC and a single dopant molecule represented as point charges in vacuum, ΔU_{ES} reduces to a simple coulomb interaction between charges. In the context of a multi-molecule system, ΔU_{ES} requires a more sophisticated treatment, which in this work is performed using an Ewald Summation.

Our expression for ΔG_{rxn} can be further simplified using the definitions of the single molecule ionization potential (IP) and electron affinity (EA).

$$\Delta G_{rxn} = IP - EA \quad (13)$$

This approximation is ubiquitous in the OSC literature. We note that IP and EA are often experimentally approximated by measuring the OSC HOMO and dopant LUMO energy levels, respectively, though the limitations of these approximations are well-documented.[46] Importantly, our formulation of the reactive MC problem for molecular doping allows one to input molecularly specific ΔG_{rxn} parameters, related to measurable redox potentials (e.g. cyclic voltammery), and couple this energetics to multi-molecule electrostatics via Equation 10. This allows for morphology changes to influence doping efficiency, and likewise for doping reactions to influence the equilibrium morphology.

To perform these MC simulations, we implemented a number of standardized techniques. Periodic boundary conditions were employed for all simulations, as well as a shifted LJ interaction cutoff radius of 2.5σ. Ewald summation is used to compute the electrostatic potential energy ($n_k = 5, \alpha = \frac{6}{L}$, where L is the box length in reduced units). Further details on parameter selection and validation can be found in the SM.

To explore how molecular phenomena govern the morphology and doping efficiency, five parameters (ΔG_{rxn}, ε, ε_{LJ}, ρ, and f_{dopant}) were explored in this study to survey a range of experimentally motivated parameters. All quantities herein are reported in reduced units, with energies scaled by the thermal energy, kT (T = 300 K) and σ_{LJ} = 1 nm. Each simulation consisted of 256 particles (unless otherwise noted), all of radius $\sigma_{LJ} = 1$ and simulated at a reduced temperature of 1 ($\sim 300K$). Simulations were equilibrated for 10^5 MC cycles, with each cycle consisting of as many MC moves as there are particles; this was observed to be substantially longer than the decorrelation times (see SM). After equilibration, sampling was performed every 100 MC cycles for 10^5 MC cycles. Each MC trajectory was initialized with only neutral OSC and dopant particles and allowed to evolve to an equilibrium doping fraction and associated morphology. Convergence of MC simulations was ascertained by monitoring the convergence of the total system energy (and its components), the dopant-dopant radial distribution function (RDF), and the doping fraction of the system with respect to the number of MC cycles. Doping fraction is quantitatively defined as the number of ionized dopants in the system divided by the total number of dopants. RDFs between OSCs and dopants are reported in the SM. Although OSC molecules are typically larger than dopant molecules, we consider equal size particles for simplicity of model validation and demonstration and to keep results agnostic to specific chemical details, as is standard in e.g. LJ fluids and restricted primitive models.

III. RESULTS AND DISCUSSION

In this work, we use the reactive MC model described in the Methods section to explore the dependence of doping efficiency on the reaction free energy (ΔG_{rxn}), system density (ρ), bulk dielectric constant (ε), and morphology of the OSC-dopant system. ΔG_{rxn} values spanned -10 kT to +10 kT, motivated by the difference in HOMO/LUMO energy levels of P3HT/F4TCNQ (0.24 eV, or 9.6 kT)[1,5,22] A positive ΔG_{rxn} value denotes that the doping direction of the ICT state reaction is endergonic. Three densities, 0.2, 0.6, and 0.8 were considered throughout the work to mimic solution and condensed phase systems. Dielectric constants of 0.05 and 1 are selected to correspond to the dielectric constants of a bulk OSC and water, respectively, to explore the influence of dielectric screening. Dopant concentration was additionally varied between 5% and 20% to be on a similar order to experimentally characterized films of polythiophenes doped with F4TCNQ.[16,17,47,48]

We first explore how doping efficiency is impacted by the ICT state reaction free energy, ΔG_{rxn}, across simulation conditions (Fig. 2). At a dielectric constant of 0.05 (equivalent to ~3-5 in real units - characteristic of most bulk OSCs), the doping efficiency is near unity, regardless of the dopant and OSC reaction energetics. While potentially surprising, such a result can be justified by considering the strength of the Coulomb interaction between an ion pair at a distance of 1σ (ε = 0.05 $\rightarrow$ ~25 kT) relative to the thermal energy at room temperature. Even provided a strongly positive ΔG_{rxn}, the magnitude of the Coulomb binding energy between the ionized products makes doping thermodynamically favorable if assuming bulk dielectric constants to be representative of local electrostatic interactions. Prior works utilizing optical near-IR absorption spectra confirm that in systems such as F4TCNQ-doped P3HT, nearly all dopants ionize,[6,49] and this evidence is

further used to inform simple analytical models of doped OSC films.[9] This result also helps rationalize the diversity of OSC-dopant chemistries in use, as such a weak influence of single molecule redox potentials on doping efficiency suggests that single molecule-derived energetic design rules are not useful rational design parameters for OSC-dopant pairs.

A richer interplay of molecular reactivity and morphology evolution is observed at a larger value of the dielectric constant. At a dielectric of $\varepsilon = 1.00$, a strong sensitivity of the doping efficiency to ΔG_{rxn} is observed (Fig. 2). Interestingly, the concentration of dopants in the simulation cell exhibits a small but significant impact on the doping efficiency, with an approximately 20% decrease in the doping efficiency manifesting when increasing dopant concentration from 5% to 20%. This effect can be related to the statistical mechanics of species in the grand canonical ensemble. Equation 10 shows that the product of prefactors including the numbers of dopants and OSCs modulates the acceptance criterion regardless of ΔG_{rxn} and, consequently, the probability of generating ionized species. The precise degree to which such an effect would manifest in an experimental OSC-dopant system is unclear, though these findings are in line with evidence from Jacobs *et al.* and Wang *et al.* that as dopant concentration increases, the fraction of dopants which ionize decreases.[5,49]

Simulations are further performed at two densities, 0.2 and 0.6, loosely corresponding to solution and semi-dilute or bulk conditions, respectively, to explore how doping efficiency is affected by the system concentration. Fig. 2 shows that density negligibly affects the doping efficiency, with higher densities exhibiting marginally higher doping efficiencies, though differences are within the error bars of the simulation. We hypothesize that this effect is also related to the prefactors of the acceptance criterion (Eqn. 10) discussed previously; for lower density (fewer number of particle) systems, these effects are more strongly magnified relative to higher densities. Consequently, the conclusion arises that doping efficiency should be only minimally affected by the density (i.e. the solvent concentration) of the OSC-dopant morphology, while exhibiting a larger (but still minor) effect related to the dopant concentration of the system. However, importantly, these effects are only observable in our simulations for a dielectric constant of 1, which is strongly screened relative to the bulk dielectric constants anticipated for OSCs. While a heterogeneous local dielectric constant deviating from the bulk value is anticipated near charged OSC-dopant pairs, our results remain an important first step in developing a molecular understanding of doping efficiency.[50]

We next explore how the variation of simulation parameters in OSC-dopant systems affect OSC-dopant morphologies. We note that the ability to explore these correlations represents a critical novelty of this work, as such a coupling of the electronic structure and morphology evolution would be prohibitively expensive over the simulated length scales for atomistic methodologies. To quantify the OSC-dopant morphology, we compute dopant-dopant RDFs (Fig. 3, Fig. 4); in this calculation all dopants, regardless of Coulombic charge, are included. At a dielectric constant of 0.05, when all dopants are ionized, the RDF has a broad peak structure that does not decay to 1 at long distances, signifying inhomogeneity indicative of dopant aggregation. Interestingly, the aggregated dopants exhibited asphericity values of approximately 0.94 for the low density simulation and 0.93 for the high density simulation, indicating that dopant aggregates are anisotropic; simulation snapshots depicted in Figures 3b and 3d corroborate this asphericity. Note that in these simulations (dielectric = 0.05) the electrostatic interactions among ionized dopants are so strong that any dependence of molecular packing structure on ΔG_{rxn} is obscured (Fig. 3a, 3c).

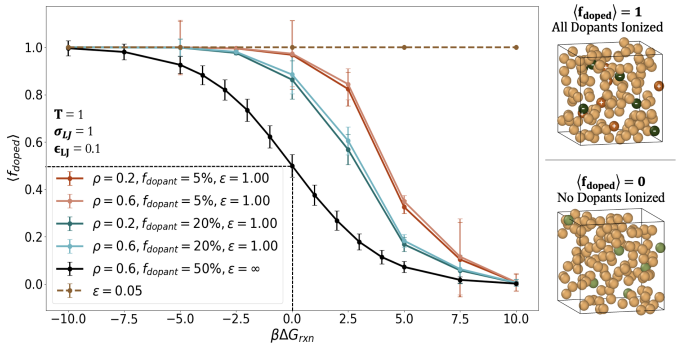

Figure 2. Doping efficiency as a function of ΔG_{rxn}. The dashed line corresponds to a simulation at a dielectric constant of 0.05. Red curves represent simulations at 5% dopant concentration (darker curves correspond to a density of 0.2), and the blue curves represent simulations at 20% dopant concentration (darker curves correspond to a density of 0.2). The black dashed line corresponds to the limit of a non-interacting mixture of 50% dopant and 50% OSCs, in which half of the dopants ionize when $\Delta G_{rxn} = 0$. Error bars represent one standard deviation of the dopant ionization fraction.

While electrostatic induced aggregation is a well-known feature of the restricted primitive model, its appearance at simulation parameters characteristic of experimental OSC-dopant systems is noteworthy. Solution-phase aggregation is a well-documented challenge of solution doping across chemical space,[5,16,20] and our results can be interpreted as such. Moreover, when coating films from doped polymer solutions, doping-induced insolubility is a common issue due to the polymer precipitating out of solution.[5,51] It has been further established that doping efficiency is controlled by the presence of these aggregates.[20,52]. Many mechanisms for doping-induced insolubility have been proposed, including a shift in the polymer dielectric and interchain interactions mediated by CTCs. However, F4TCNQ-doped P3HT demonstrates this insolubility despite low dielectric solvents and predominantly ICT state generation; thus, it has been proposed that doping-induced insolubility results from the stabilization of holes in solvochromic polymers. The energy difference between a hole on an unaggregated polymer versus an aggregated polymer could induce aggregation if the stabilization overcomes the Coulombic repulsion between holes and the polymer solvation energy.[5,53] The mechanistic explanation here is simply that in low dielectric solvents electrostatic interactions are strong enough to promote near unity doping, and thus induce aggregation. This amounts to what is effectively reaction-

induced phase separation.

To further explore reaction-induced effects on the OSC-dopant morphology, we performed simulations at a dielectric constant of 1, where effective electrostatic interactions are weak (Fig. 4). Dopant-dopant RDFs look significantly more like homogeneous liquids (Fig. 4a, 4c), and significant control over the dopant-dopant RDF structure is induced by changing the reaction free energy (ΔG_{rxn}) of the system. As ΔG_{rxn} is reduced, more dopants ionize and the repulsive interactions between negatively charged dopants reduce the density of dopants in the first solvation shell. Most notably, reaction-induced aggregation no longer occurs, even at the most exothermic ΔG_{rxn} values, where all dopants are ionized (Fig. 3b, 3d). This result provides further evidence that the strength of the Coulombic interactions between ions drives reaction-induced aggregation in OSC-dopant systems. When the dopant and OSCs are uncharged, the system is homogeneous (i.e. it is soluble; Fig. 4b, d), and as the simulation progresses the dopants and OSCs become charged, and segregation of the morphology occurs (Fig. 3b, d). Experimental literature has established that aggregation can be tuned by solvent choice; a common example involves the comparison of thiophene films in acetonitrile and chlorobenzene.[16] In principle, the lower dielectric constant of acetonitrile may enhance the stabilizing electrostatic contribution and eventual clustering of ions, while the higher dielectric constant of chlorobenzene is associated with a more homogeneous distribution of dopants. Solvents should be chosen with caution, as their energetic interactions with the dopant and OSC play an influential role in modulating electrostatic interactions, which in turn governs a variety of molecular packing structures.

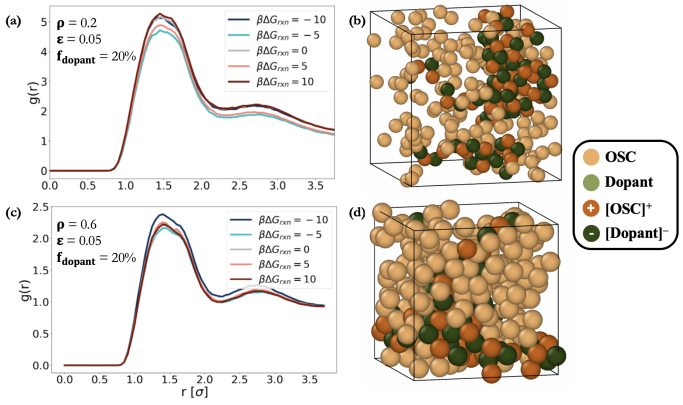

Figure 3. Dopant-dopant radial distribution functions (RDFs) at low dielectric for two simulation densities. The broad peak in the RDF tail at densities of 0.2 (a) and 0.6 (c) indicates dopant aggregation when electrostatic interactions among ionized dopants are strong ($\varepsilon = 0.05$). Representative simulation snapshots corresponding to (a) and (c) are shown in (b) and (d), respectively. Orange particles represent OSCs (light orange for neutral particles and dark orange for cations) and green particles represent dopants (light green for neutral particles and dark green for anions).

To further investigate how dopant aggregation influences doping efficiency, different sizes of dopant clusters were introduced into a system where a total of 512 particles were

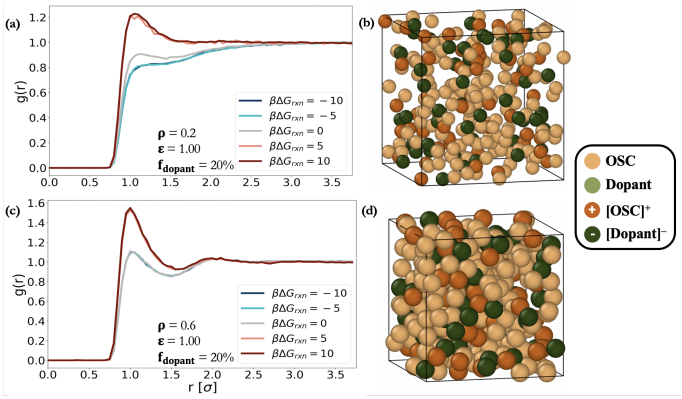

Figure 4. Dopant-dopant radial distribution functions (RDFs) at high dielectric for two simulation densities. Weakened electrostatic interactions result in RDFs resembling homogeneous liquids, with tails approaching 1 at large distances. Representative simulation snapshots corresponding to (a) and (c) are shown in (b) and (d), respectively. Orange particles represent OSCs (light orange for neutral particles and dark orange for cations) while green particles represent dopants (light green for neutral particles and dark green for anions).

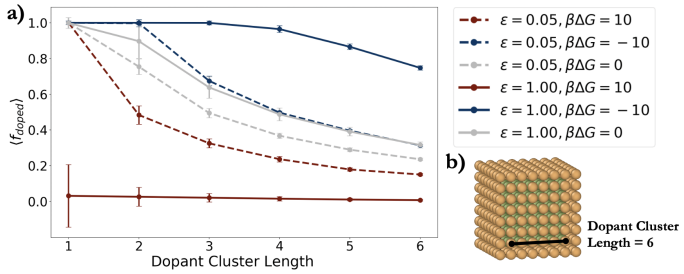

Figure 5. The effect of dopant aggregate size on doping efficiency. (a) Doping efficiency as a function of cluster size assuming a simple cubic morphology of dopant and OSC. Error bars represent the standard deviation of dopant ionization fraction across the MC trajectory. Snapshot (b) visualizes cluster lengthscale.

fixed on a 8x8x8 cubic lattice for the duration of the simulation. For reference, dopant cubes of side length 3, 4, and 5 roughly correspond to concentrations of 5, 12.5, and 25 percent, respectively. Each of these systems was simulated using three ΔG_{rxn} values and at dielectric constant values of 0.05 and 1.00 (Fig. 5). For a given set of parameters, the size of the cluster could cause up to an 80% decrease in doping efficiency (as in the ε = 0.05, ΔG_{rxn} = 10 case) relative to the homoegeneous system. The system with the lowest doping efficiency is a high ΔG_{rxn} and high dielectric, which is consistent with expected trends of dielectric and ΔG_{rxn}. Interestingly, the system that has the highest doping efficiency occurs when ΔG_{rxn} is low and surprisingly, the dielectric constant is high. In fact, the expectation that a lower dielectric constant would lead to a higher doped fraction is only observed in the case of a large free energy barrier (ΔG_{rxn} = 10 kT). We speculate that in the case of a low ΔG_{rxn} where there is a strong driving force to ionize (i.e. ΔG_{rxn} = -10), this propensity is counterbalanced by dopants being in a clustered state

where like-charges are very close together and thus repulsive interactions dominate potential energy. Our findings illustrate that not only do electrostatic interactions drive the equilibrium morphology as shown in Figure 3 and Figure 4, but the morphology drives the possible electrostatic interactions,[43,51] with some non-intutive relationships emerging. Importantly, these simulations show that dopant aggregation can play a significant role in shifting the balance between ΔG_{rxn} and dielectric, and this complex interplay will be of key importance for the molecular design of OSC-dopant systems.

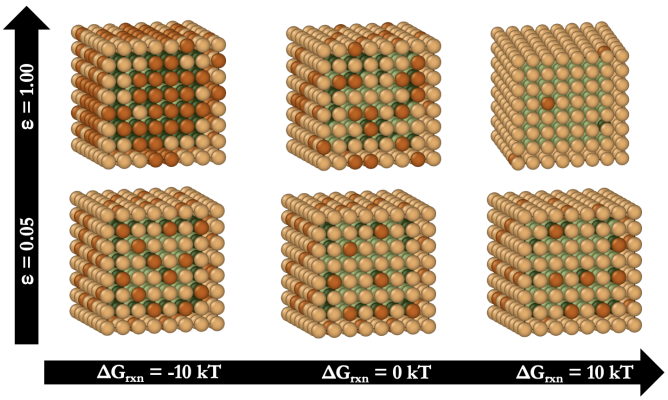

Figure 6. Simulation snapshots depicting the spatial distribution of charges as a function of two dielectric constants and three ΔG_{rxn} values for a centrally located cube of 216 dopants within a 512 particle lattice.

While these estimated doping efficiencies provide a quantitative sense of the extent of ionization in the system, simulation snapshots from the 6x6x6 dopant cluster case across all simulation conditions shed further insight into how the charges are distributed on the cubic cluster. At a dielectric of 1.00 (specifically, the ΔG_{rxn} = -10 kT and ΔG_{rxn} = 0 kT case), the electrostatic screening enables charged dopant particles to closely pack, leading to the higher doping efficiency stipulated earlier. Additionally, these snapshots confirm that only the dopants on the surface of the cluster ionize due to the stabilization energy of a nearby OSC ion. This further justifies the dramatic impact film morphology and heterogeneity may have in doped OSC films. A brief discussion of how the doping efficiency is affected if the clusters were not fixed to a lattice, and rather able to evolve and rearrange is provided in the Supplementary Materials, but we note that experimental films with OSC molecules are typically kinetically arrested morphologies due to high glass transition temperatures not captured by our MC simulations.

Computational modelling for integrated OSC-dopant design requires simultaneously reconciling local electronic structure and film morphology across multiple length and time scales. In this work, we have developed a simple but powerful simulation approach for coupling chemically specific reaction energetics with morphology evolution, facilitating the exploration of doping-induced morphology evolution, dopant structuring, and doping efficiency. Provided the broad diversity of dopant chemistries in the experimental literature, we see the simplicity of the proposed model as a benefit that provides simple physical insights into molecular doping using easily controllable parameters such as the dielectric constant (ε), mutual dopant-OSC solubility (ε_{LJ}), dopant size (σ_{LJ}), and the density (ρ) and composition (f_{dopant}) of the system. While the forms of our parameters, potential functions, and physical approximations are simple, our approach can be further enhanced by incorporating more complex phenomena which distinguish doped OSC systems from other molecular systems.

The reactive MC model used in this work is limited in the complexity of quantum mechanical charge states it can incorporate. At present, our reactive MC model only incorporates integer charge transfer events, though delocalized charge transfer events (including CTC state formation) are known to play a role in doped OSC performance and system design.[1,22,24–26,35,54] To incorporate more complex physics associated with the hybridization of dopant-OSC orbitals and charge delocalization within the OSC domains, extensions to the reactive MC framework are required. As experimental doping efficiencies are known to be strongly influenced by the strength of electrostatic interactions between charged species, the presence of fractional charges (i.e. CTC states) would constitute a dramatic reduction in the strength of these interactions. Similarly, the delocalization of charge throughout OSC domains would present another physically sensible mechanism for reducing the strength of Coulombic interactions.[55] However, as the integration of a continuum of delocalized reaction states into reaction MC represents a challenging and, to our knowledge, unexplored methodological approach, it will require careful consideration and derivation of the appropriate move proposals, acceptance criteria, and calculation of molecular parameters. Specifically, coupling these move proposals with a quantum mechanically faithful model Hamiltonian could allow for a rigorous incorporation of the physics of electron delocalization into our simulation framework. Such further development of the reactive MC model shown here could demonstrate how the equilibrium of different dopant states interplays with the complexities of the multiscale morphology, directly accessing the morphology-dependence of the relative distribution of ICT and CTC states that has been the target of many experimental works in recent years.

Another important limitation of our model is the fundamentally treatment of doping. As the acceptance of MC moves in any molecular simulation is dictated by thermodynamic probabilities, kinetics are absent. While the exclusion of kinetics provides obvious benefits in terms of the equilibration of the morphology that for glassy systems in particular can be quite crucial, little work has been performed to explore the morphology-dependence of doping kinetics in molecularly doped systems. These considerations motivate the quantum chemical analysis of electron transfer rates in molecularly doped systems using simple model chemistries; such approaches proliferate the organic photovoltaics literature and have been critical for understanding the ultrafast nature of charge separation.[56,57] Interestingly, the dopants designed by Spokoyny benefit from large, sterically inhibiting and non-conductive dopant regions that likely suppress charge recombination rates.[4,58,59] To incorporate kinetic effects into our re-

active MC framework would be challenging, but kinetic MC approaches are well-known in the literature and could be reasonably incorporated into our model.[60–64]

As the model in this work has been intentionally coarse-grained with the hope of understanding the general physics of molecular doping in OSC films, the limitations of such coarse-grained models for capturing crucial chemical specificity are well-known and can be incorporated in future works. Notably, atomistic or quantum mechanical treatments will provide significantly more accurate characterizations of electrostatic interactions, polarization, effective local dielectric constants, and quantum mechanical delocalization of charge carriers, but will exhibit significant computational cost increases that will inhibit accessible simulation length scales. Likely the most important correction to our present model can involve a more sophisticated treatment of the local dielectric functions, particularly as a function of local charging due to doping reactions. The sensitivity of CG simulation results to the value of the effective dielectric constant is a well-known computational result, particularly in the polyelectrolyte modeling literature.[65,66] Recent work in molecular dopants has shown that the dielectric constant as a function of doping can be manipulated to induce dramatic performance changes,[50] making this a critical consideration for future efforts. Lastly, the isotropic nature of our interaction potentials, while potentially reasonable for many molecular dopants, is likely untenable for OSCs that are known to exhibit strong anisotropic packing. The existence of anisotropic models for molecular and polymeric systems are well-known and could be adapted to improve chemical fidelity at reduced computational cost.[29,67,68]

IV. CONCLUSION

We have developed a simple but powerful approach to describing doping reaction-induced morphology changes in molecularly doped systems using Reactive MC. This study represents the first work, to our knowledge, capable of coupling the details of the doping reaction energetics to morphology evolution, with the potential for computational scalability and chemically generalizable insights. These simulations reveal that doping efficiency is controlled by the organic semiconductor's dielectric constant, with near unit doping efficiency occurring in any well-mixed film morphology. In many observed simulations, we find doping reaction-induced aggregation, which we link to the known difficulty of solution deposition of organic semiconductors and dopants simultaneously. Importantly, we explicitly quantify the ability of dopant aggregates to reduce the overall doping efficiency of the film by more than 50%. This result reinforces the commonly observed experimental trend of working to ensure the homogeneous dispersion of molecular dopants throughout the organic semiconductor film. This work represents an important first step towards the systematic integration of molecular electronic structure and mesoscopic morphology evolution into the characterization of multi-scale structure-function relationships in molecularly doped OSCs.

ACKNOWLEDGMENTS

N.E.J. acknowledges support by the Office of Naval Research under grant number N00014-23-1-2542. A.V. acknowledges that this material is based upon work supported by the National Science Foundation Graduate Research Fellowship Program under Grant No. DGE 21-46756.

DATA AVAILABILITY STATEMENT

The data that support the findings of this study are available from the corresponding author upon reasonable request.

REFERENCES

[1] Henry Méndez, Georg Heimel, Stefanie Winkler, Johannes Frisch, Andreas Opitz, Katrein Sauer, Berthold Wegner, Martin Oehzelt, Christian Röthel, Steffen Duhm, Daniel Többens, Norbert Koch, and Ingo Salzmann. Charge-transfer crystallites as molecular electrical dopants. *Nature Communications*, 6, 10 2015.

[2] Eric Daniel Głowacki, Gundula Voss, and Niyazi Serdar Sariciftci. 25th anniversary article: Progress in chemistry and applications of functional indigos for organic electronics. *Advanced Materials*, 25(47):6783–6800, 12 2013.

[3] Bernard Geffroy, Philippe le Roy, and Christophe Prat. Organic light-emitting diode (OLED) technology: Materials, devices and display technologies, 6 2006.

[4] Alberto D. Scaccabarozzi, Aniruddha Basu, Filip Aniés, Jian Liu, Osnat Zapata-Arteaga, Ross Warren, Yuliar Firdaus, Mohamad Insan Nugraha, Yuanbao Lin, Mariano Campoy-Quiles, Norbert Koch, Christian Müller, Leonidas Tsetseris, Martin Heeney, and Thomas D. Anthopoulos. Doping Approaches for Organic Semiconductors, 2021.

[5] Ian E. Jacobs and Adam J. Moulé. Controlling Molecular Doping in Organic Semiconductors, 11 2017.

[6] P. Pingel and D. Neher. Comprehensive picture of p-type doping of P3HT with the molecular acceptor F4TCNQ. *Physical Review B - Condensed Matter and Materials Physics*, 87(11), 3 2013.

[7] Martin Schwarze, Christopher Gaul, Reinhard Scholz, Fabio Bussolotti, Andreas Hofacker, Karl Sebastian Schellhammer, Bernhard Nell, Benjamin D. Naab, Zhenan Bao, Donato Spoltore, Koen Vandewal, Johannes Widmer, Satoshi Kera, Nobuo Ueno, Frank Ortmann, and Karl Leo. Molecular parameters responsible for thermally activated transport in doped organic semiconductors. *Nature Materials*, 18(3), 2019.

[8] V. I. Arkhipov, E. V. Emelianova, P. Heremans, and H. Bässler. Analytic model of carrier mobility in doped disordered organic semiconductors. *Physical Review B - Condensed Matter and Materials Physics*, 72(23), 12 2005.

[9] V I Arkhipov, Paul Heremans, E V Emelianova, and Heinz Baessler. Effect of doping on the density-of-states distribution and carrier hopping in disordered organic semiconductors. *Physical Review B*, 71(4):45214, 2005.

[10] Wenrui Zhao, Jiamin Ding, Ye Zou, Chong An Di, and Daoben Zhu. Chemical doping of organic semiconductors for thermoelectric applications. *Chemical Society Reviews*, 49(20):7210–7228, 10 2020.

[11] G. H. Kim, L. Shao, K. Zhang, and K. P. Pipe. Engineered doping of organic semiconductors for enhanced thermoelectric efficiency. *Nature Materials*, 12(8):719–723, 8 2013.

[12] B. Lüssem, M. Riede, and K. Leo. Doping of organic semiconductors, 1 2013.

[13] Ingo Salzmann, Georg Heimel, Martin Oehzelt, Stefanie Winkler, and Norbert Koch. Molecular Electrical Doping of Organic Semiconductors: Fundamental Mechanisms and Emerging Dopant Design Rules. *Accounts of Chemical Research*, 49(3):370–378, 2 2016.

[14] Kristen E. Watts, Bharati Neelamraju, Maximilian Moser, Iain McCulloch, Erin L. Ratcliff, and Jeanne E. Pemberton. Thermally Induced Formation of HF4TCNQ-in F4TCNQ-Doped Regioregular P3HT. *Journal of Physical Chemistry Letters*, 11(16):6586–6592, 8 2020.

[15] Massimiliano Comin, Vincent Lemaur, Andrea Giunchi, David Beljonne, Xavier Blase, and Gabriele D'avino. Doping of semicrystalline conjugated polymers: dopants within alkyl chains do it better †. *J. Mater. Chem. C*, 10:13815, 2022.

[16] Ian E Jacobs, Erik W Aasen, Julia L Oliveira, Tayane N Fonseca, John D Roehling, Jun Li, Gwangwu Zhang, Matthew P Augustine, Mark Mascal, and Adam J Moulé. Comparison of solution-mixed and sequentially processed P3HT:F4TCNQ films: effect of doping-induced aggregation on film morphology †.

[17] Mark F. DiTusa, Garrett L. Grocke, Tengzhou Ma, and Shrayesh N. Patel. Probing the evolution of conductivity and structural changes in vapor-F4TCNQ doped P3HT. *Molecular Systems Design and Engineering*, 7(7):788–797, 4 2022.

[18] Justin E Cochran, Matthias J N Junk, Anne M Glaudell, P Levi Miller, John S Cowart, Michael F Toney, Craig J Hawker, Bradley F Chmelka, and Michael L Chabinyc. Molecular interactions and ordering in electrically doped polymers: blends of PBTTT and F4TCNQ. *Macromolecules*, 47(19):6836–6846, 2014.

[19] Henry Méndez, Georg Heimel, Andreas Opitz, Katrein Sauer, Patrick Barkowski, Martin Oehzelt, Junshi Soeda, Toshihiro Okamoto, Jun Takeya, Jean Baptiste Arlin, Jean Yves Balandier, Yves Geerts, Norbert Koch, and Ingo Salzmann. Doping of organic semiconductors: Impact of dopant strength and electronic coupling. *Angewandte Chemie - International Edition*, 52(30):7751–7755, 7 2013.

[20] Jian Gao, Edwards T Niles, and John K Grey. Aggregates promote efficient charge transfer doping of poly (3-hexylthiophene). *The Journal of Physical Chemistry Letters*, 4(17):2953–2957, 2013.

[21] Duc T Duong, Chenchen Wang, Erin Antono, Michael F Toney, and Alberto Salleo. The chemical and structural origin of efficient p-type doping in P3HT. *Organic Electronics*, 14(5):1330–1336, 2013.

[22] Eric Chih-Kuan Wu, Charlene Z Salamat, Sarah H Tolbert, and Benjamin J Schwartz. Molecular Dynamics Study of the Thermodynamics of Integer Charge Transfer vs Charge-Transfer Complex Formation in Doped Conjugated Polymers. *Cite This: ACS Appl. Mater. Interfaces*, 14, 2022.

[23] Ian E Jacobs, Camila Cendra, Thomas F Harrelson, Zaira I Bedolla Valdez, Roland Faller, Alberto Salleo, and Adam J Moulé. Polymorphism controls the degree of charge transfer in a molecularly doped semiconducting polymer. *Materials Horizons*, 5(4):655–660, 2018.

[24] Ana M Valencia and Caterina Cocchi. Electronic and optical properties of oligothiophene-f4tcnq charge-transfer complexes: The role of the donor conjugation length. *The Journal of Physical Chemistry C*, 123(14):9617–9623, 2019.

[25] Dane A Stanfield, Yutong Wu, Sarah H Tolbert, and Benjamin J Schwartz. Controlling the Formation of Charge Transfer Complexes in Chemically Doped Semiconducting Polymers. 2021.

[26] Bharati Neelamraju, Kristen E. Watts, Jeanne E. Pemberton, and Erin L. Ratcliff. Correlation of Coexistent Charge Transfer States in F 4 TCNQ-Doped P3HT with Microstructure. *Journal of Physical Chemistry Letters*, 9(23):6871–6877, 12 2018.

[27] Riccardo Alessandri, Jaakko J. Uusitalo, Alex H. De Vries, Remco W.A. Havenith, and Siewert J. Marrink. Bulk Heterojunction Morphologies with Atomistic Resolution from Coarse-Grain Solvent Evaporation Simulations. *Journal of the American Chemical Society*, 139(10):3697–3705, 3 2017.

[28] David M. Huang, Roland Faller, Khanh Do, and Adam J. Moule. Coarse-grained computer simulations of polymer/fullerene bulk heterojunctions for organic photovoltaic applications. *Journal of Chemical Theory and Computation*, 6(2):526–537, 2 2010.

[29] Alexander E Cohen, Nicholas E Jackson, and Juan J De Pablo. Anisotropic coarse-grained model for conjugated polymers: investigations into solution morphologies. *Macromolecules*, 54(8):3780–3789, 2021.

[30] Nicholas E. Jackson. Coarse-Graining Organic Semiconductors: The Path to Multiscale Design. *The Journal of Physical Chemistry B*, 125(2):485–496, 12 2021.

[31] Shuichi Nagamatsu and Shyam S. Pandey. Ordered arrangement of F4TCNQ anions in three-dimensionally oriented P3HT thin films. *Scientific Reports*, 10(1), 12 2020.

[32] Jenny Nelson, Joe J. Kwiatkowski, James Kirkpatrick, and Jarvist M. Frost. Modeling charge transport in organic photovoltaic materials. *Accounts of Chemical Research*, 42(11):1768–1778, 11 2009.

[33] Eric C. Wu and Benjamin J. Schwartz. Does the Traditional Band Picture Describe the Electronic Structure of Doped Conjugated Polymers? TD-DFT and Natural Transition Orbital Study of Doped P3HT. *Journal of Chemical Theory and Computation*, 19(19):6761–6769, 10 2023.

[34] Ana M Valencia, Michele Guerrini, and Caterina Cocchi. Ab initio modelling of local interfaces in doped organic semiconductors †. *Phys. Chem. Chem. Phys*, 22:3527, 2020.

[35] Osnat Zapata-Arteaga, Bernhard Dörling, Aleksandr Perevedentsev, Jaime Martín, J. Sebastian Reparaz, and Mariano Campoy-Quiles. Closing the Stability-Performance Gap in Organic Thermoelectrics by Adjusting the Partial to Integer Charge Transfer Ratio. *Macromolecules*, 53(2):609–620, 1 2020.

[36] J. Karl Johnson, Athanassios Z. Panagiotopoulos, and Keith E. Gubbins. Reactive canonical monte carlo a new simulation technique for reacting or associating fluids. *Molecular Physics*, 81(3), 1994.

[37] W. R. Smith and B. Triska. The reaction ensemble method for the computer simulation of chemical and phase equilibria. I. Theory and basic examples. *The Journal of Chemical Physics*, 100(4):3019–3027, 1994.

[38] Anshul D S Parmar, Benjamin Guiselin, and Ludovic Berthier. Stable glassy configurations of the Kob-Andersen model using swap Monte Carlo. *J. Chem. Phys*, 153:134505, 2020.

[39] Anshul D S Parmar, Misaki Ozawa, and Ludovic Berthier. Ultrastable Metallic Glasses In Silico. *Physical Review Letters*, 125, 2020.

[40] Chad R Snyder and Dean M Delongchamp. Glassy phases in organic semiconductors.

[41] Lingyun Zhu, Eung Gun Kim, Yuanping Yi, and Jean Luc Brédas. Charge transfer in molecular complexes with 2,3,5,6-tetrafluoro-7,7,8,8-tetracyanoquinodimethane (F4-TCNQ): A density functional theory study. *Chemistry of Materials*, 23(23):5149–5159, 12 2011.

[42] Patrick Pingel, Lingyun Zhu, Kue Surk Park, Jörn Oliver Vogel, Silvia Janietz, Eung Gun Kim, Jürgen P. Rabe, Jean Luc Brédas, and Norbert Koch. Charge-transfer localization in molecularly doped thiophene-based donor polymers. *Journal of Physical Chemistry Letters*, 1(13):2037–2041, 7 2010.

[43] Hannes Hase, Melissa Berteau-Rainville, Somaiyeh Charoughchi, Wolfgang Bodlos, Emanuele Orgiu, and Ingo Salzmann. Critical dopant concentrations govern integer and fractional charge-transfer phases in doped P3HT. *JPhys Materials*, 6(1), 1 2023.

[44] Tomá S Grigera and Giorgio Parisi. Fast Monte Carlo algorithm for supercooled soft spheres.

[45] Daan Frenkel and Berend Smit. *Understanding molecular simulation: from algorithms to applications*. Academic Press, San Deigo, 2002.

[46] Brett M. Savoie, Nicholas E. Jackson, Tobin J. Marks, and Mark A. Ratner. Reassessing the use of one-electron energetics in the design and characterization of organic photovoltaics. *Physical Chemistry Chemical Physics*, 15(13):4538–4547, 4 2013.

[47] Duo Liu, Jun Hang Li, Si Chun Wang, Lu Zhang, Xin Yu Liu, Qiang Zhang, and Yan Chun Han. Control Aggregation of P3HT in Solution for High Efficiency Doping: Ensuring Structural Order and the Distribution of Dopants. *Chinese Journal of Polymer Science (English Edition)*, 5 2023.

[48] Kelly A Peterson, Ashlea Patterson, Alejandro Vega-Flick, Bolin Liao, and Michael L Chabinyc. Doping molecular organic semiconductors by diffusion from the vapor phase †. *Mater. Chem. Front*, 4:3632, 2020.

[49] Chenchen Wang, Duc T. Duong, Koen Vandewal, Jonathan Rivnay, and Alberto Salleo. Optical measurement of doping efficiency in poly(3-hexylthiophene) solutions and thin films. *Physical Review B - Condensed Matter and Materials Physics*, 91(8), 2 2015.

[50] Massimiliano Comin, Simone Fratini, Xavier Blase, and Gabriele D'Avino. Doping-Induced Dielectric Catastrophe Prompts Free-Carrier Release in Organic Semiconductors. *Advanced Materials*, 34(2), 1 2022.

[51] Kan Tang, Frederick M Mcfarland, Skye Travis, Jasmine Lim, Jason D Azoulay, and Song Guo. Aggregation of P3HT as a preferred pathway for its chemical doping with F 4-TCNQ †. *Chem. Commun*, 54:11925, 2018.

[52] Julie Euvrard, Amélie Revaux, Pierre Alain Bayle, Michel Bardet, Dominique Vuillaume, and Antoine Kahn. The formation of polymer-dopant aggregates as a possible origin of limited doping efficiency at high dopant concentration. *Organic Electronics*, 53:135–140, 2 2018.

[53] Jack Fuzell, Ian E. Jacobs, Sophia Ackling, Thomas F. Harrelson, David M. Huang, Delmar Larsen, and Adam J. Moulé. Optical Dedoping Mechanism for P3HT:F4TCNQ Mixtures. *Journal of Physical Chemistry Letters*, 7(21):4297–4303, 11 2016.

[54] Kristen E. Watts, Bharati Neelamraju, Erin L. Ratcliff, and Jeanne E. Pemberton. Stability of Charge Transfer States in F4TCNQ-Doped P3HT. *Chemistry of Materials*, 31(17):6986–6994, 9 2019.

[55] Brett M. Savoie, Akshay Rao, Artem A. Bakulin, Simon Gelinas, Bijan Movaghar, Richard H. Friend, Tobin J. Marks, and Mark A. Ratner. Unequal partnership: Asymmetric roles of polymeric donor and fullerene acceptor in generating free charge. *Journal of the American Chemical Society*, 136(7):2876–2884, 2 2014.

[56] M Mandel and T Odijk. Dielectric Properties Of Polyelectrolyte Solutions. Technical report, 1984.

[57] Tao Liu and Alessandro Troisi. Absolute rate of charge separation and recombination in a molecular model of the P3HT/PCBM interface. *Journal of Physical Chemistry C*, 115(5):2406–2415, 2 2011.

[58] Taylor J. Aubry, K. J. Winchell, Charlene Z. Salamat, Victoria M. Basile, Jeffrey R. Lindemuth, Julia M. Stauber, Jonathan C. Axtell, Rebecca M. Kubena, Minh D. Phan, Matthew J. Bird, Alexander M. Spokoyny, Sarah H. Tolbert, and Benjamin J. Schwartz. Tunable Dopants with Intrinsic Counterion Separation Reveal the Effects of Electron Affinity on Dopant Intercalation and Free Carrier Production in Sequentially Doped Conjugated Polymer Films. *Advanced Functional Materials*, 30(28), 7 2020.

[59] Taylor J. Aubry, Jonathan C. Axtell, Victoria M. Basile, K. J. Winchell, Jeffrey R. Lindemuth, Tyler M. Porter, Ji Yuan Liu, Anastassia N. Alexandrova, Clifford P. Kubiak, Sarah H. Tolbert, Alexander M. Spokoyny, and Benjamin J. Schwartz. Dodecaborane-Based Dopants Designed to Shield Anion Electrostatics Lead to Increased Carrier Mobility in a Doped Conjugated Polymer. *Advanced Materials*, 31(11), 3 2019.

[60] Reinder Coehoorn, Harm Van Eersel, Peter A. Bobbert, and René A.J. Janssen. Kinetic Monte Carlo Study of the Sensitivity of OLED Efficiency and Lifetime to Materials Parameters. *Advanced Functional Materials*, 25(13):2024–2037, 4 2015.

[61] Jacob T. Willson, William Liu, Daniel Balzer, and Ivan Kassal. Jumping Kinetic Monte Carlo: Fast and Accurate Simulations of Partially Delocalized Charge Transport in Organic Semiconductors. *Journal of Physical Chemistry Letters*, 14(15):3757–3764, 4 2023.

[62] Daniel Balzer, Thijs J A M Smolders, David Blyth, Samantha N Hood, and Ivan Kassal. Delocalised kinetic Monte Carlo for simulating delocalisation-enhanced charge and exciton transport in disordered materials. 2021.

[63] N. J. van der Kaap and L. J.A. Koster. Massively parallel kinetic Monte Carlo simulations of charge carrier transport in organic semiconductors. *Journal of Computational Physics*, 307:321–332, 2 2016.

[64] Robin G E Kimber, Edward N Wright, Simon E J O'kane, Alison B Walker, and James C Blakesley. Mesoscopic kinetic Monte Carlo modeling of organic photovoltaic device characteristics. *Physical Review B*, 86:235206, 2012.

[65] J. J. Cerdà, B. Qiao, and Ch Holm. Modeling strategies for polyelectrolyte multilayers. *European Physical Journal: Special Topics*, 177(1):129–148, 10 2009.

[66] Jiaxing Yuan, Hanne S. Antila, and Erik Luijten. Dielectric Effects on Ion Transport in Polyelectrolyte Brushes. *ACS Macro Letters*, 8(2):183–187, 2 2019.

[67] David M. Friday and Nicholas E. Jackson. Electron and ion transport in semi-dilute conjugated polyelectrolytes: view from a coarse-grained tight binding model. *Molecular Systems Design and Engineering*, 8(6):743–755, 2 2023.

[68] David M. Friday and Nicholas E. Jackson. Modeling the Interplay of Conformational and Electronic Structure in Conjugated Polyelectrolytes. *Macromolecules*, 55(5):1866–1877, 3 2022.